Numerical Simulation of Solitary-Wave Scattering and Damping in Fragmented Sea Ice

Philippe Guyenne[1], Emilian I. Părău[2]

[1] Department of Mathematical Sciences, University of Delaware, Newark, DE 19716, USA
[2] School of Mathematics, University of East Anglia, Norwich, NR4 7TJ, UK

ABSTRACT

A numerical model for direct phase-resolved simulation of nonlinear ocean waves propagating through fragmented sea ice is proposed. In view are applications to wave propagation and attenuation across the marginal ice zone. This model solves the full equations for nonlinear potential flow coupled with a nonlinear thin-plate formulation for the ice cover. Distributions of ice floes can be directly specified in the physical domain by allowing the coefficient of flexural rigidity to be spatially variable. Dissipation due to ice viscosity is also taken into account by including diffusive terms in the governing equations. Two-dimensional simulations are performed to examine the attenuation of solitary waves by scattering and damping through an irregular array of ice floes. Wave attenuation over time is quantified for various floe configurations.

KEY WORDS: flexural-gravity waves; ice floes; scattering; solitary waves; spectral method; viscosity; wave attenuation.

INTRODUCTION

The rapid decline of summer ice extent that has occurred in the Arctic Ocean over recent years has prompted a surge of research activity and, in particular, the role of ocean waves in controlling sea-ice morphology has been increasingly recognized. This is especially relevant in the context of climate change as the resulting ice melting and proliferation of open water promote further wave growth over increasing fetches, thus allowing long waves to propagate larger distances into the ice field. Of particular interest is the marginal ice zone (MIZ) which is the fragmented part of the ice cover closest to the open ocean and, as such, it is a very dynamic region strongly affected by incoming ocean waves. By breaking up the sea ice, waves cause it to become more fragmented, which in turn increases their capacity to further penetrate and damage the ice cover. Unfortunately, such information has not been factored into previous climate predictions and this is now becoming a pressing issue. State-of-the-art forecasting models of wind-driven gravity waves are only beginning to be tested with crude parameterizations for wave-ice interactions (Doble and Bidlot, 2013).

While the problem of ocean waves interacting with sea ice has drawn attention for some time now, the vast majority of theoretical studies have used linear approximations of the governing equations. In view is the description of wave attenuation through ice-covered seas. This direction of inquiry has produced an abundant literature and has reached a high degree of sophistication spanning a variety of situations. For the MIZ, two different approaches have commonly been adopted: (*i*) continuum models for waves propagating through an inhomogeneous ice cover described as a uniform material with effective properties including viscosity or viscoelasticity (Wang and Shen, 2010; Zhao et al, 2015), and (*ii*) separate-floe models where the ice cover is composed of individual floes with possibly different characteristics (Kohout and Meylan, 2008; Bennetts and Squire, 2009). Unlike case (*i*) that includes dissipative processes, case (*ii*) focuses on wave attenuation by scattering (i.e. directional spreading) through the heterogeneous ice field. Indeed, measurements from Wadhams et al (1988) provided evidence that wave scattering by ice floes is the dominant mechanism for energy attenuation in the MIZ. In case (*i*), an explicit formula for the linear dispersion relation can be derived and can provide a theoretical basis for subgrid parameterizations in wave forecasting models. Case (*ii*) leads to solving a mixed boundary value problem where quantities measuring the degree of wave reflection and transmission can be determined. Theoretical predictions based on scattering theory typically give an exponential decay of linear waves with distance traveled through sea ice (Bennetts and Squire, 2012).

Despite some progress in recent years, the nonlinear theory is still in its infancy. A body of work has focused on the analysis and simulation of flexural-gravity waves in continuous uniform sea ice, and has employed thin-plate theory (Euler–Bernoulli theory when strains are finite and/or infinitesimal) for the ice combined with nonlinear potential-flow theory for the fluid. Results include weakly nonlinear modeling in various asymptotic regimes as well as direct numerical simulation (Părău and Dias, 2002; Milewski et al, 2011; Guyenne and Părău, 2015). Numerical and theoretical results on nonlinear waves propagating in fragmented sea ice are even more scarce, and this largely remains an open problem. An attempt has been made by e.g. Hegarty and Squire (2008) who devised a boundary integral method to compute the perturbative second-order solution for the problem of large-amplitude ocean waves interacting with a compliant floating raft such as an ice floe.

In the present paper, we describe a numerical model recently proposed by Guyenne and Părău (2017), which allows for phase-resolved simulation of nonlinear ocean waves propagating through fragmented sea ice. This approach is based on the full time-dependent equations for nonlinear potential flow and can directly incorporate spatial distributions of ice floes. The ice cover is viewed as an elastic material according to the special Cosserat theory of hyperelastic shells (Plotnikov and Toland, 2011), with an ad-hoc modification to define its spatial dependence. This

micropolar theory was selected to form the basis for our ice-cover model because it combines a number of compelling features: it is nonlinear, conservative and well suited to direct numerical simulation. In particular, it fits well within the commonly used Hamiltonian formulation for ocean waves (Zakharov, 1968). Restricting our attention to the two-dimensional finite-depth problem with solitary waves as incident wave conditions, we present extended results on wave attenuation by scattering and damping through an irregular array of ice floes. In particular, an original contribution of this paper is the inclusion of dissipative effects due to ice viscosity in the model. Their significance relative to scattering effects is examined via direct numerical simulations.

In the following sections, we introduce the mathematical formulation of this hydroelastic problem, including the model for fragmented sea ice and for ice viscosity. We then describe the numerical methods to efficiently and accurately solve the resulting equations. Finally, we show numerical results on wave attenuation for various floe configurations. These results are discussed with respect to such parameters as incident wave amplitude, ice concentration and ice fragmentation.

MATHEMATICAL FORMULATION

Equations of Motion

The basic mathematical formulation that we use is for a two-dimensional fluid of uniform finite depth h beneath a continuous ice sheet of infinite horizontal extent. The fluid is assumed to be incompressible, inviscid and the flow to be irrotational. The ice sheet is modeled as a thin elastic plate according to the special Cosserat theory of hyperelastic shells in Cartesian coordinates (x, y), with the horizontal x-axis being the bottom of the ice sheet at rest and the y-axis directed vertically upwards (Plotnikov and Toland, 2011). The vertical deformation of the ice is denoted by $y = \eta(x, t)$. The fluid velocity potential $\Phi(x, y, t)$ satisfies the Laplace equation

$$\nabla^2 \Phi = 0, \quad \text{for} \quad x \in \mathbb{R}, \quad -h < y < \eta(x, t). \tag{1}$$

The nonlinear boundary conditions at $y = \eta(x, t)$ are the kinematic condition

$$\eta_t + \Phi_x \eta_x = \Phi_y, \tag{2}$$

and the dynamic (or Bernoulli) condition

$$\Phi_t + \frac{1}{2}|\nabla\Phi|^2 + g\eta + \frac{\sigma}{\rho}\left(\kappa_{ss} + \frac{1}{2}\kappa^3\right) = 0, \tag{3}$$

where the subscripts are shorthand notation for partial derivatives (e.g. $\Phi_t = \partial_t\Phi$), κ is the mean curvature of the fluid-ice interface and s is the arclength along this interface. In terms of η, the mean curvature is given by

$$\kappa = \frac{\eta_{xx}}{(1+\eta_x^2)^{3/2}},$$

and the nonlinear bending force exerted by the ice sheet onto the fluid surface reads

$$\kappa_{ss} + \frac{1}{2}\kappa^3 = \frac{1}{2}\left(\frac{\eta_{xx}}{(1+\eta_x^2)^{3/2}}\right)^3 + \frac{1}{\sqrt{1+\eta_x^2}}\partial_x\left[\frac{1}{\sqrt{1+\eta_x^2}}\partial_x\left(\frac{\eta_{xx}}{(1+\eta_x^2)^{3/2}}\right)\right].$$

This system of equations is completed with the condition at the bottom,

$$\Phi_y = 0, \quad \text{at} \quad y = -h. \tag{4}$$

The constant σ is the coefficient of flexural rigidity for the ice sheet, $\rho = 1025$ kg/m^3 is the fluid density and $g = 9.8$ m/s^2 is the acceleration due to gravity. Since the wavelengths being considered are much larger than the ice thickness, we neglect the inertia of the thin ice sheet, hence the plate acceleration term is not included here. We also assume that the elastic plate is inextensible and not pre-stressed, and the tension due to plate stretching and bending is negligible. The coefficient of flexural rigidity is defined by

$$\sigma = \frac{E\ell^3}{12(1-\nu^2)},$$

where $E = 6$ GPa and $\nu = 0.3$ denote Young's modulus and Poisson's ratio for the ice respectively, and ℓ is its average thickness.

Dirichlet–Neumann Operator

Following Guyenne and Părău (2012, 2014), we can reduce the dimensionality of the Laplace problem (1)~(4) by introducing $\xi(x, t) = \Phi(x, \eta(x, t), t)$, the trace of the velocity potential on $y = \eta(x, t)$, together with the Dirichlet–Neumann operator (DNO)

$$G(\eta)\xi = (-\eta_x, 1)^\top \cdot \nabla\Phi\big|_{y=\eta},$$

which is the singular integral operator that takes Dirichlet data ξ on $y = \eta(x, t)$, solves the Laplace equation (1) for Φ subject to (4), and returns the corresponding Neumann data (i.e. the normal fluid velocity there).

In terms of these boundary variables, the equations of motion (2) and (3) take the form

$$\eta_t = G(\eta)\xi, \tag{5}$$

$$\xi_t = -\frac{1}{2(1+\eta_x^2)}\left[\xi_x^2 - (G(\eta)\xi)^2 - 2\xi_x\eta_xG(\eta)\xi\right] \\ -g\eta - \frac{\sigma}{\rho}\left(\kappa_{ss} + \frac{1}{2}\kappa^3\right), \tag{6}$$

which is a closed system for η and ξ, extending Zakharov's formulation for water waves ($\sigma = 0$) to ice-covered ocean waves ($\sigma \neq 0$). Dissipative effects have so far been ignored.

In light of its analyticity properties with respect to η (Coifman and Meyer, 1985), the DNO can be expressed in terms of a convergent Taylor series expansion

$$G(\eta) = \sum_{j=0}^{\infty} G_j(\eta), \tag{7}$$

where each term G_j can be determined recursively (Craig and Sulem, 1993). More specifically, for even $j = 2r > 0$,

$$G_{2r}(\eta) = \frac{1}{(2r)!}G_0(|D|^2)^{r-1}D\eta^{2r}D \tag{8}$$
$$-\sum_{s=0}^{r-1}\frac{1}{(2(r-s))!}(|D|^2)^{r-s}\eta^{2(r-s)}G_{2s}(\eta)$$
$$-\sum_{s=0}^{r-1}\frac{1}{(2(r-s)-1)!}G_0(|D|^2)^{r-s-1}\eta^{2(r-s)-1}G_{2s+1}(\eta),$$

and, for odd $j = 2r - 1 > 0$,

$$G_{2r-1}(\eta) = \frac{1}{(2r-1)!}(|D|^2)^{r-1}D\eta^{2r-1}D \tag{9}$$
$$-\sum_{s=0}^{r-1}\frac{1}{(2(r-s)-1)!}G_0(|D|^2)^{r-s-1}\eta^{2(r-s)-1}G_{2s}(\eta)$$
$$-\sum_{s=0}^{r-2}\frac{1}{(2(r-s-1))!}(|D|^2)^{r-s-1}\eta^{2(r-s-1)}G_{2s+1}(\eta),$$

where $D = -i\partial_x$ and $G_0 = D\tanh(hD)$ are Fourier multiplier operators (D is defined in such a way that its Fourier symbol is k and thus $|D|$ corresponds to $|k|$). In the infinite-depth limit ($h \to \infty$), G_0 reduces to $|D|$.

This series expansion of the DNO provides an efficient elliptic solver that will be exploited in the present numerical study. Such a formulation involving boundary variables alone has been successfully used in other contexts, e.g. in perturbation calculations for surface gravity waves in single- and double-layer fluids (Craig et al, 2009, 2010, 2012), as well as in direct numerical simulations with uniform or variable water depth (Guyenne and Nicholls, 2007; Xu and Guyenne, 2009; Guyenne et al, 2010).

Model for Fragmented Sea Ice

Equations (5) and (6) describing wave propagation in a continuous ice sheet will form the basis for our model of fragmented sea ice. We will extend this continuum formulation in an ad-hoc manner to model the combined effects of two distinct mechanisms that contribute to wave attenuation in the MIZ: scattering through an irregular array of separate floes and dissipation due to ice viscosity.

As proposed by Guyenne and Părău (2017), a spatial distribution of ice floes can be directly specified in the physical domain by allowing the coefficient of flexural rigidity to be a variable function in space, namely $f(x)\sigma/\rho$, whose amplitude varies between 0 (open water) and σ/ρ (pack ice). Such a way of manipulating the bending force is similar to the approach of Williams and Squire (2004) who described heterogeneities (e.g. pressure ridges) in a continuous ice sheet by making the coefficient of flexural rigidity spatially dependent.

In our two-dimensional procedure for generating a fragmented ice cover of total length L_c, we first prescribe a regular array of N_f identical floes whose individual length is L_f and which are evenly distributed over the distance L_c. Then, to make this arrangement look more irregular (and thus more realistic), each floe is shifted by an amount $\theta L_f/2$ relative to its initial center of gravity, where θ is a random number uniformly distributed between -1 and 1. Occasionally, if two neighboring floes happen to overlap after this shift, the resulting longer floe will further contribute to inhomogeneity of the simulated ice cover. At the edges of each floe, the continuous transition between the two phases (from ice to water or vice versa) should be made steep but smooth enough to clearly distinguish the individual floes while complying with the continuum character of the underlying formulation. We typically use a tanh-like profile for this phase transition.

Figure 1 illustrates one realization of the spatial function $f(x)$ for the coefficient of flexural rigidity over the entire domain $[0, L] = [0, 600]$. In this example, the ice field consists of $N_f = 5$ floes of individual length $L_f = 60$, as represented by the plateaux $f(x) = 1$, which are randomly positioned over the interval $[100, 100 + L_c] = [100, 500]$. Because they are required to lie within $[100, 500]$, those which have been shifted outside this range are cut off (like the last floe in Fig. 1 which has been shifted too much to the right by the randomization procedure). There is no feedback mechanism from floes to waves in our formulation, so the ice floes are not allowed to drift and their number is not allowed to vary during the time evolution.

Dissipation due to ice viscosity is modeled by adding linear diffusive terms to (5) and (6), with a coefficient of viscosity being proportional to $f(x)$ so that wave damping via this mechanism effectively takes place in the presence of ice. Our motivation for using this viscous model is twofold. First, it is sufficiently simple that it can be easily incorporated into the underlying formulation and thus is well suited to direct numerical simulation, as advocated in the next section. Second, it is analogous to
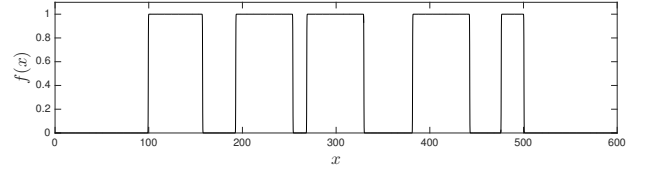

Figure 1: One realization of the spatial variation $f(x)$ for the coefficient of flexural rigidity. The ice cover spans a distance $L_c = 400$ between $x = 100$ and $x = 500$, and consists of $N_f = 5$ floes whose individual length is specified to be $L_f = 60$.

Dias et al (2008)'s model for weakly damped free-surface flows where dissipation is due to water viscosity. In that context, viscous corrections to the potential-flow equations also take the form of diffusive terms.

We point out that continuum viscoelastic-type models for wave-ice interactions in the MIZ are more empirical than the present model in the sense that their rheological parameters (including the viscosity parameter) do not correspond to specific properties of sea ice but rather they are meant to represent wave attenuation from various sources combined. By contrast here, we clearly distinguish conservative mechanisms (i.e. scattering caused by ice floes) from non-conservative mechanisms and, concerning the latter, we only examine dissipation due to ice viscosity. It would be possible to include other dissipative processes by redefining the coefficient of viscosity but this will not be considered in the present study.

The new equations of motion read

$$\eta_t = G(\eta)\xi + 2\frac{\lambda}{\rho}f(x)\eta_{xx}, \tag{10}$$

$$\xi_t = -\frac{1}{2(1+\eta_x^2)}\left[\xi_x^2 - (G(\eta)\xi)^2 - 2\xi_x\eta_x G(\eta)\xi\right]$$
$$-g\eta - \frac{\sigma}{\rho}f(x)\left(\kappa_{ss} + \frac{1}{2}\kappa^3\right) + 2\frac{\lambda}{\rho}f(x)\xi_{xx} + P, \tag{11}$$

where λ denotes the dynamic viscosity of ice and P represents any other possible forces acting at the top boundary. Note that, for simplicity, we slightly deviate from Dias et al (2008)'s formulation who proposed a viscous term proportional to Φ_{yy} on the left-hand side of (3) and, instead, we replace it by

$$-\Phi_{yy}\big|_{y=\eta} \simeq \xi_{xx},$$

on the right-hand side of (11). Otherwise, when reduced to boundary variables, this term would yield more contributions depending on the DNO and its derivatives. Such a simplification is consistent with the thin-plate approximation for the ice sheet and leads to diffusive terms similar to those used in e.g. eddy-viscosity models for breaking waves (Tian and Choi, 2013). It would be of interest to include the full expression of Φ_{yy} in (11) and test its performance in the future.

DIRECT NUMERICAL SIMULATIONS

In this section, we describe the numerical methods to efficiently and accurately solve the full system of equations (10)$\sim$(11). These methods deal with the spatial discretization as well as the temporal integration to allow for direct simulations in the time domain. We then present numerical results on the attenuation of solitary waves in fragmented sea ice. Both effects of scattering and dissipation are examined.

Numerical Methods

For space discretization, we assume periodic boundary conditions in x (with $0 \leq x \leq L$) and use a pseudo-spectral method based on the fast Fourier transform (FFT). This is a particularly suitable choice for computing the DNO since each term in its Taylor series (7) consists of concatenations of Fourier multipliers with powers of η.

More specifically, both functions η and ξ are expanded in truncated Fourier series

$$\left(\begin{array}{c} \eta \\ \xi \end{array} \right) = \sum_k \left(\begin{array}{c} \widehat{\eta}_k \\ \widehat{\xi}_k \end{array} \right) e^{ikx}.$$

Spatial derivatives and Fourier multipliers are evaluated in the Fourier space, while nonlinear products are calculated in the physical space on a regular grid of N collocation points. For example, if we wish to apply the zeroth-order operator G_0 to a function ξ in the physical space, we transform ξ to the Fourier space, apply the diagonal operator $k\tanh(hk)$ to the Fourier coefficients $\widehat{\xi}_k$, and then transform back to the physical space.

In practice, the Taylor series of the DNO is also truncated to a finite number of terms,

$$G(\eta) \approx G^M(\eta) = \sum_{j=0}^{M} G_j(\eta), \tag{12}$$

but thanks to its analyticity properties, a small number of terms (typically $M < 10$) are sufficient to achieve highly accurate results (Xu and Guyenne, 2009). The computational cost for evaluating (12) is estimated to be $O(M^2 N \log N)$ via the FFT. Aliasing errors are removed by zero-padding in the Fourier space.

Time integration of (10) and (11) is performed in the Fourier space so that linear terms can be solved exactly by the integrating factor technique. For this purpose, we separate the linear terms with constant coefficients from the nonlinear terms and linear terms with variable coefficients. Setting $v = (\eta, \xi)^\top$, these equations can be expressed as

$$v_t = \mathscr{L}v + \mathscr{N}(v), \tag{13}$$

where the linear part $\mathscr{L}v$ is defined by

$$\mathscr{L}v = \left(\begin{array}{cc} 0 & G_0 \\ -g & 0 \end{array} \right) \left(\begin{array}{c} \eta \\ \xi \end{array} \right),$$

and the remaining part $\mathscr{N}(v)$ is given by $\mathscr{N}(v) = (\mathscr{N}_1, \mathscr{N}_2)^\top$ with

$$\mathscr{N}_1 = [G(\eta) - G_0]\xi + 2\frac{\lambda}{\rho}f(x)\eta_{xx},$$

$$\mathscr{N}_2 = -\frac{1}{2(1+\eta_x^2)}\left[\xi_x^2 - (G(\eta)\xi)^2 - 2\xi_x\eta_x G(\eta)\xi \right]$$
$$- \frac{\sigma}{\rho}f(x)\left(\kappa_{ss} + \frac{1}{2}\kappa^3 \right) + 2\frac{\lambda}{\rho}f(x)\xi_{xx} + P.$$

Via the change of variables

$$\widehat{v}_k(t) = \Theta(t)\widehat{w}_k(t),$$

in the Fourier space, involving

$$\Theta(t) = \left(\begin{array}{cc} \cos\left(t\sqrt{gG_0}\right) & \sqrt{\frac{G_0}{g}}\sin\left(t\sqrt{gG_0}\right) \\ -\sqrt{\frac{g}{G_0}}\sin\left(t\sqrt{gG_0}\right) & \cos\left(t\sqrt{gG_0}\right) \end{array} \right),$$

system (13) takes the form

$$\partial_t \widehat{w}_k = \Theta(t)^{-1}\widehat{\mathscr{N}_k}\left[\Theta(t)\widehat{w}_k\right],$$

which only contains terms from $\mathscr{N}$ and is solved numerically in time using the fourth-order Runge–Kutta scheme with constant step Δt. By converting back to $\widehat{v}_k$, this scheme reads

$$\widehat{v}_k^{n+1} = \Theta(\Delta t)\widehat{v}_k^n + \frac{\Delta t}{6}\Theta(\Delta t)\left(f_1 + 2f_2 + 2f_3 + f_4 \right), \tag{14}$$

where

$$f_1 = \widehat{\mathscr{N}_k}(\widehat{v}_k^n),$$

$$f_2 = \Theta\left(-\frac{\Delta t}{2}\right)\widehat{\mathscr{N}_k}\left[\Theta\left(\frac{\Delta t}{2}\right)\left(\widehat{v}_k^n + \frac{\Delta t}{2}f_1 \right) \right],$$

$$f_3 = \Theta\left(-\frac{\Delta t}{2}\right)\widehat{\mathscr{N}_k}\left[\Theta\left(\frac{\Delta t}{2}\right)\left(\widehat{v}_k^n + \frac{\Delta t}{2}f_2 \right) \right],$$

$$f_4 = \Theta(-\Delta t)\widehat{\mathscr{N}_k}\left[\Theta(\Delta t)\left(\widehat{v}_k^n + \Delta t f_3 \right) \right],$$

for the solution at time $t_{n+1} = t_n + \Delta t$. The integrating factor $\Theta(t)$ is the fundamental matrix of the linear system $\partial_t \widehat{v}_k = \mathscr{L}\widehat{v}_k$ and, in the limit $k \to 0$, it reduces to

$$\Theta(t) = \left(\begin{array}{cc} 1 & 0 \\ -gt & 1 \end{array} \right).$$

To obtain (14), we use the fact that $\Theta(t)$ is a semigroup satisfying

$$\Theta(a+b) = \Theta(a)\Theta(b), \qquad \Theta(a)^{-1} = \Theta(-a).$$

These identities can be easily checked by direct calculation. Despite being linear, the diffusive terms are not included in $\mathscr{L}$ and $\Theta(t)$ because their coefficient is spatially variable. From the pseudo-spectral perspective, these terms are evaluated in the same way as a nonlinear product.

Expectedly, the scattering by ice floes was found to produce small-amplitude short waves that radiate backwards from the main pulse but these tend to contaminate the advancing solution by re-entering the computational domain from the other end due to the periodic boundary conditions. To overcome this difficulty, we specify a sponge layer by including a damping pressure term of the form

$$P = -\frac{\delta(x)G(\eta)\xi}{\sqrt{1+\eta_x^2}},$$

on the right-hand side of (11), where $\delta(x)$ is a tunable spatially dependent coefficient that is nonzero only in a small region near each end of the domain and away from the ice floes. A tanh-like profile is also used to represent the localized spatial behavior of $\delta(x)$.

Numerical Results

For convenience, Eqs. (10)∼(11) are non-dimensionalized using the characteristic scales

$$\left(\frac{\sigma}{\rho g}\right)^{1/4}, \quad \left(\frac{\sigma g^3}{\rho}\right)^{1/8},$$

as unit length and unit speed respectively. This implies that the coefficients g and σ/ρ are scaled out of the equations, while the coefficient of ice viscosity takes the dimensionless form

$$\gamma = \frac{\lambda}{\rho}\left(\frac{\rho^3}{\sigma^3 g}\right)^{1/8}.$$

We set $\gamma = 5 \times 10^{-4}$ as a representative value based on the choice $\lambda = 31$ Pa · s and $\ell = 0.4$ m (Newyear and Martin, 1997). In the following, we

will retain the original notation for the physical variables but the reader should keep in mind that these now refer to dimensionless quantities.

Incident wave conditions are given by solitary waves that solve the basic equations (1)~(4) for surface gravity waves ($\sigma = 0$). We focus on the shallow-water (or long-wave) regime that is characterized by pure solitary waves with a single localized hump. Such solutions are computed by a boundary integral method based on Cauchy's integral formula and have been extensively tested via time-dependent simulations using our spectral scheme (Craig et al, 2006). In the absence of ice, they propagate steadily without change of shape and speed, and may be viewed as a prototype for long swell waves. We set $h = 1$ to be the reference unit length scale.

In our simulations, we typically use $\Delta t = 0.002$ (with $M = 6$) as a good compromise between accuracy, stability and computational cost. As a reference, this time step is hundreds times smaller than the linear wave period in shallow water $\tau = \sqrt{h/g} = 1$ for $h = 1$. Given the fourth-order accuracy of our time-integration scheme, this value of Δt is quite reasonable. The choice $M = 6$ for the truncation order of the DNO is motivated by previous tests on surface gravity waves and flexural-gravity waves along a continuous ice sheet, where it has been found to yield highly accurate results at a moderate cost (Guyenne and Părău, 2014).

The present setup features a domain of length $L = 1200$, with the fragmented ice cover lying between $x = 100$ and $x = 1100$ (hence $L_c = 1000$). The main objective is to quantify the attenuation of solitary waves propagating over this distance, as a function of incident wave height A, ice concentration $C \simeq N_f L_f / L_c$ and ice fragmentation $F \simeq N_f$. The quantities $N_f L_f / L_c$ and N_f should be viewed as average values of C and F since their exact values may slightly vary from one realization to another due to floe merging and trimming by the randomization procedure.

To quantify this attenuation, we use the L^2 norm

$$\|\eta\|_2 = \left(\frac{1}{L}\int_0^L \eta(x,t)^2 \mathrm{d}x\right)^{1/2}, \quad (15)$$

which denotes the standard deviation relative to the zero mean value of η (i.e. the quiescent level). Equation (15) is a measure of dispersion (i.e. loss of coherency) of the solitary wave. The smaller this L^2 norm, the closer the solution to a small-amplitude dispersive wave with zero mean value. The integral in (15) is evaluated numerically by the trapezoidal rule.

We consider realizations from four different floe configurations defined by $(N_f, L_f) = (77, 4)$, $(77, 8)$, $(13, 60)$, $(13, 72)$ and corresponding to average ice concentrations $C = 0.31$, 0.62, 0.78, 0.94 respectively. Among them, two pairs of configurations display well distinct ice fragmentations: one pair $(N_f, L_f) = (77, 4)$ and $(77, 8)$ is particularly fragmented, composed of many small floes, while the other pair $(N_f, L_f) = (13, 60)$ and $(13, 72)$ is less fragmented, consisting of much fewer but larger floes. Each pair has two configurations with varying floe sizes, hence varying ice concentrations, but L_f was not varied too much in order to ensure a certain level of ice fragmentation and avoid the risk of excessive floe merging by the randomization procedure. Typically, the larger N_f and L_f (i.e. the higher C), the closer the floe configuration to a continuous ice sheet. Among these four configurations, the case $(N_f, L_f) = (77, 4)$ is closest to open-water conditions since it has the lowest C and highest F, while the case $(N_f, L_f) = (13, 72)$ is most similar to a continuous ice sheet since it has the highest C and lowest F.

Because special attention is paid to nonlinear wave effects, we choose to examine a fairly large amplitude $A = 0.3$ (relative to $h = 1$) as an illustrative example. This incident wave amplitude is six times bigger than the (dimensionless) ice thickness $\ell = 0.05$. A peculiarity of solitary waves is that the higher the amplitude, the more localized the pulse and expectedly the more pronounced the attenuation in the presence of ice.
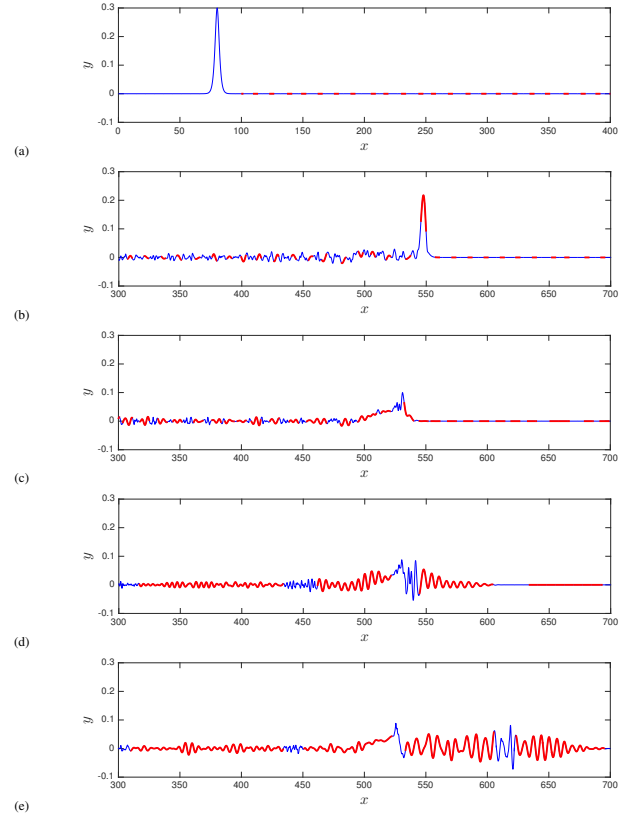

Figure 2: Snapshots of η for $(N_f, L_f) = (77, 4)$ at $t = 0$ (a), $(77, 4)$ at $t = 416$ (b), $(77, 8)$ at $t = 416$ (c), $(13, 60)$ at $t = 416$ (d) and $(13, 72)$ at $t = 416$ (e) with $A = 0.3$ in the non-viscous case. Open water is represented in blue color while ice floes are represented in red color.

Therefore, $A = 0.3$ is a suitable choice for our study of wave scattering and damping in fragmented sea ice.

First, we investigate the role of wave scattering caused by ice floes and disregard ice viscosity by setting $\gamma = 0$. To show what the attenuation process and various floe configurations look like in the physical space, Fig. 2 provides snapshots of η at a few instants during wave propagation across the ice field. A single realization of each of the floe settings is considered and, for graphical purposes, the individual floes are associated with the values of $f(x) \in [1-\varepsilon, 1+\varepsilon]$ (with $\varepsilon = 10^{-3}$) to take floating-point arithmetic into account. The incident solitary wave is initially located at $x = 80$ near the left edge of the ice cover, and travels from left to right. Its interaction with the random array of ice floes gives rise to an irregular pattern of wave scattering whose characteristics and associated wave decay depend on the levels of C and F.

Figure 2 suggests that two distinct mechanisms coexist and contribute to wave attenuation: (i) multiple wave reflections from the ice floes (most apparent in the short-floe configurations) and (ii) pulse spreading due to the presence of ice itself (most apparent in the long-floe configurations). Case (i) produces small backward radiation while case (ii) can generate a moderately large dispersive wave train that propagates forward ahead of the main pulse. In all cases however, we can discern a remnant of the initial solitary wave, which persists throughout the entire propagation. For the sparsest floe configuration $(N_f, L_f) = (77, 4)$, the solitary wave is seen to travel essentially unaffected aside from a slight decrease in amplitude. By contrast, for $(N_f, L_f) = (77, 8)$, the incident
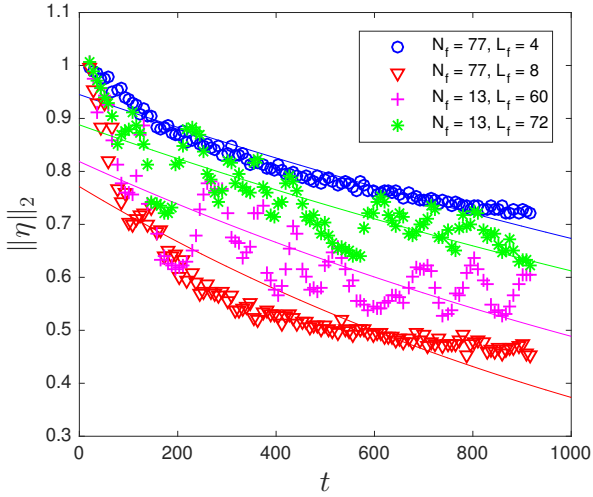
Figure 3: L^2 norm of η as a function of time for $A = 0.3$ in the non-viscous case. Numerical data are represented in various symbols while their exponential fits are plotted in solid line.

Figure 4: L^2 norm of η as a function of time for $A = 0.3$ in floe configuration $(N_f, L_f) = (77,4)$ (a), $(77,8)$ (b), $(13,60)$ (c) and $(13,72)$ (d). Comparison between the viscous and non-viscous cases is shown.

wave quickly decays through backward radiation and pulse spreading while retaining a well-localized shape. In this case, the maximum wave elevation gets as low as $\eta_{max} \simeq 0.05$ (which is comparable to ℓ) at $t = 950$ when the main pulse reaches the right edge of the ice field. These results indicate that the ice cover should be sufficiently fragmented and dense for wave attenuation to be significant, with a floe size on the order of the wavelength or pulse extent.

To further quantify the observed attenuation, Fig. 3 depicts the L^2 norm (15) as a function of time for all four floe settings. These numerical data span a long time interval $t \in (0, 1000) \gg \tau$ and are normalized relative to the incident values at $t = 0$. Motivated by linear predictions, the least-squares exponential fit

$$\|\eta\|_2 = \beta e^{\alpha t}, \tag{16}$$

to each data set is also presented in this figure as a reference. Although we look at wave characteristics as functions of time, there is a direct correspondence with the behavior as a function of distance traveled into the ice field owing to the localized and progressive nature of solitary waves. Figure 3 confirms that $(N_f, L_f) = (77,4)$ and $(77,8)$ are the least and most attenuating floe configurations, respectively, among the four considered. Because $(N_f, L_f) = (77,8)$ defines a highly fragmented ice cover, multiple wave reflections caused by ice floes likely plays a major role in wave attenuation. However, as mentioned above, its level of ice concentration is such that the mechanism of pulse spreading also contributes to wave scattering and helps make the whole process more effective.

While the exponential fit (16) performs reasonably well for $(N_f, L_f) = (77,4)$ when the attenuation is weak, it provides a poorer approximation to the numerical data when the attenuation is stronger. This is especially apparent in the case $(N_f, L_f) = (77,8)$ and the reason is because the data seem to converge to a nonzero (positive) limit rather than to zero as time goes on. Guyenne and Pǎrǎu (2017) found that a two-term exponential function of the form

$$\|\eta\|_2 = \beta_1 e^{\alpha_1 t} + \beta_2 e^{\alpha_2 t},$$

where α_1 and α_2 are of opposite signs, provides a better fit. Consistent with previous observations from Fig. 2, this stagnating behavior as $t \to$
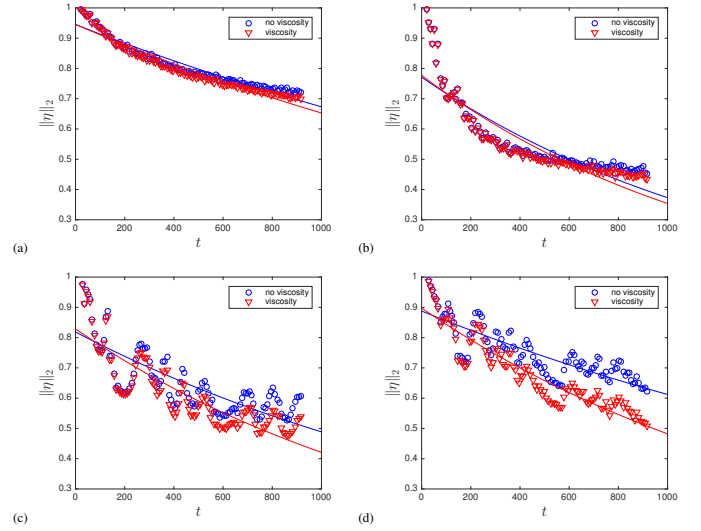
$+\infty$ may be attributed in part to the well-known stability of solitary waves (Benjamin, 1972), which prevents them from completely disintegrating as they travel across the ice field.

We now incorporate ice viscosity ($\gamma = 5 \times 10^{-4}$) and compare the L^2 results with those obtained in the previous non-viscous case ($\gamma = 0$) for $A = 0.3$. The graphs are shown in Fig. 4 for all four floe settings. We see that viscous effects may be significant, especially in long-floe configurations where ice concentration is high thus allowing such effects to accumulate over time. For the short-floe setting $(N_f, L_f) = (77,8)$ where strong attenuation takes place through wave scattering, the correction due to viscous damping is found to be relatively small. But overall, the presence of ice viscosity tends to induce a faster decay rate as expected.

To further explore the dependence of wave attenuation on physical parameters, we extract the exponential decay rate α from L^2 data in the non-viscous case. This decay rate is plotted as a function of incident wave conditions and floe parameters in Fig. 5. Because a wider range of $A = \{0.01, 0.02, 0.05, 0.1, 0.2, 0.3\}$ is examined, which implies a higher computational cost, we consider a smaller domain of length $L = 600$ with $L_c = 400$ for this calculation. Accordingly, while the same values of L_f are used to define the four floe configurations, the corresponding values of N_f are now smaller. Looking at Fig. 5, the tendency for wave scattering and attenuation (i.e. $\alpha < 0$) is confirmed in all cases. The larger the incident wave amplitude, the faster the decay rate (i.e. $|\alpha|$ increases with A), and scattering effects are negligible for $A = 0.01$ and $A = 0.02$. This is a consequence of the pulse being more localized as A is increased, which approximates shorter waves experiencing more scattering. It is also clearly demonstrated that $(N_f, L_f) = (31,8)$ is significantly more favorable to wave attenuation than $(N_f, L_f) = (5,60)$ although they display similar levels of C. Given that the floe configuration $(N_f, L_f) = (31,8)$ is much more fragmented than $(N_f, L_f) = (5,60)$ while being even slightly less concentrated in ice, i.e. $C = 0.61$ and $C = 0.66$ respectively, this clearly indicates that wave scattering is promoted by a high level of F.
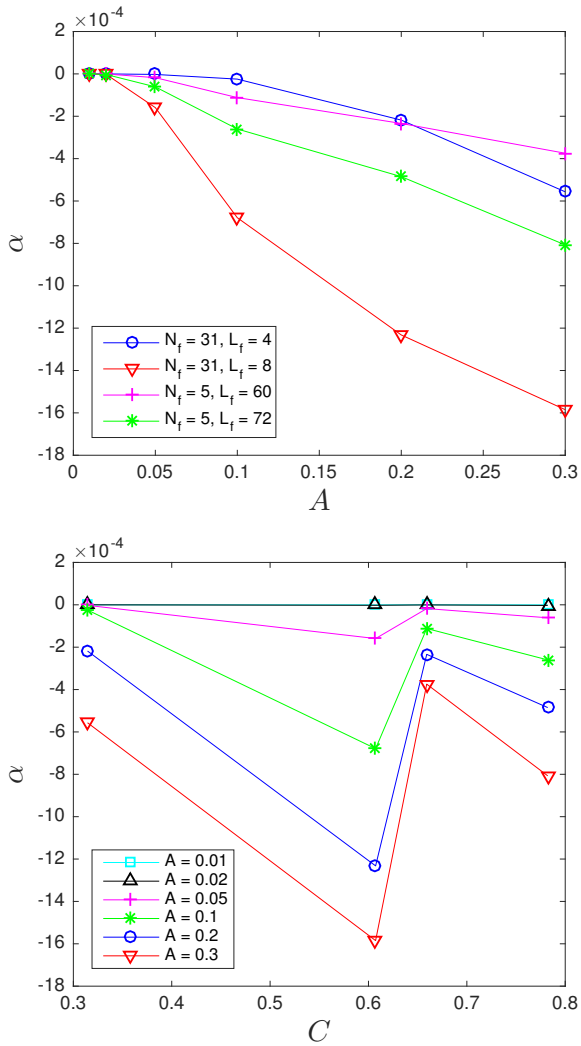
Figure 5: Exponential rate of attenuation for the L^2 norm of η as a function of A (upper panel) and C (lower panel) in the non-viscous case.

CONCLUSIONS

We have proposed a numerical model for direct phase-resolved simulation of nonlinear ocean waves interacting with fragmented sea ice. This approach is based on the full time-dependent equations for nonlinear potential flow, combined with a thin-plate model for the ice cover according to the special Cosserat theory of hyperelastic shells. Via an ad-hoc extension of the original plate formulation, spatial distributions of ice floes can be directly incorporated into the numerical algorithm to mimick sea-ice morphology in the MIZ. We have also explored the possibility of including diffusive terms in the equations of motion to model dissipation due to ice viscosity.

Restricting our attention to the two-dimensional finite-depth problem, we have examined the attenuation of solitary waves due to scattering and damping through an irregular array of ice floes. The numerical model was run for various floe configurations, and the L^2 norm of η was used to quantify this attenuation over time as a function of incident wave height, ice concentration and ice fragmentation. Our main results can be summarized as follows. (i) The larger the incident wave amplitude, the stronger the attenuation, which is a consequence of the more localized profile of the pulse and is consistent with linear predictions and field observations (Wadhams et al, 1988). (ii) The most attenuating floe configuration represents a good compromise between ice concentration and ice fragmentation such that both mechanisms of pulse spreading and multiple wave reflections contribute to wave attenuation in an effective way. (iii) The inclusion of ice viscosity may have significant dissipative effects on wave dynamics over time, especially in long-floe configurations where ice concentration is high.

The present model should be viewed as a first step to provide a platform for direct phase-resolved simulation of nonlinear ocean waves in the MIZ. In the future, we plan to investigate the three-dimensional problem with fragmented sea ice and compare with recent field measurements (Meylan et al, 2014). The proposed approach for simulating wave-ice interactions is readily extensible to three dimensions. Preliminary three-dimensional computations were performed by Părău and Vanden-Broeck (2011) for nonlinear potential flow coupled with a continuous ice sheet according to linear Euler–Bernoulli theory.

REFERENCES

Benjamin, TB (1972). "The stability of solitary waves," *Proc R Soc Lond A*, 328, 153-183.

Bennetts, LG, and Squire, VA (2009). "Wave scattering by multiple rows of circular ice floes," *J Fluid Mech*, 639, 213-238.

Bennetts, LG, and Squire, VA (2012). "On the calculation of an attenuation coefficient for transects of ice-covered ocean," *Proc R Soc A*, 468, 136-162.

Coifman, R, and Meyer, Y (1985). "Nonlinear harmonic analysis and analytic dependence," *Proc Symp Pure Math*, 43, 71-78.

Craig, W, Guyenne, P, Hammack, J, Henderson, D, and Sulem, C (2006). "Solitary water wave interactions," *Phys Fluids*, 18, 057106.

Craig, W, Guyenne, P, and Sulem, C (2009). "Water waves over a random bottom," *J Fluid Mech*, 640, 79-107.

Craig, W, Guyenne, P, and Sulem, C (2010). "A Hamiltonian approach to nonlinear modulation of surface water waves," *Wave Motion*, 47, 552-563.

Craig, W, Guyenne, P, and Sulem, C (2012). "The surface signature of internal waves," *J Fluid Mech*, 710, 277-303.

Craig, W, and Sulem, C (1993). "Numerical simulation of gravity waves," *J Comp Phys*, 108, 73-83.

Dias, F, Dyachenko, AI, and Zakharov, VE (2008). "Theory of weakly damped free-surface flows: A new formulation based on potential flow solutions," *Phys Lett A*, 372, 1297-1302.

Doble, MJ, and Bidlot, J-R (2013). "Wavebuoy measurements at the Antarctic sea ice edge compared with an enhanced ECMWF WAM: progress towards global waves-in-ice modeling," *Ocean Model*, 70, 166-173.

Guyenne, P, Lannes, D, and Saut, J-C (2010). "Well-posedness of the Cauchy problem for models of large amplitude internal waves," *Nonlinearity*, 23, 237-275.

Guyenne, P, and Nicholls, DP (2007). "A high-order spectral method for nonlinear water waves over moving bottom topography," *SIAM J Sci Comp*, 30, 81-101.

Guyenne, P, and Părău, EI (2012). "Computations of fully nonlinear hydroelastic solitary waves on deep water," *J Fluid Mech*, 713, 307-329.

Guyenne, P, and Părău, EI (2014). "Finite-depth effects on solitary waves in a floating ice sheet," *J Fluids Struct*, 49, 242-262.

Guyenne, P, and Părău, EI (2014). "Forced and unforced flexural-gravity solitary waves," *Procedia IUTAM*, 11, 44-57.

Guyenne, P, and Părău, EI (2015). "Asymptotic modeling and numerical simulation of solitary waves in a floating ice sheet," *Proc 25th Int Ocean and Polar Eng Conf*, Kona, ISOPE, 467-475.

Guyenne, P, and Părău, EI (2017). "Numerical study of solitary wave attenuation in a fragmented ice sheet," submitted.

Hegarty, GM, and Squire, VA (2008). "A boundary-integral method for the interaction of large-amplitude ocean waves with a compliant floating raft such as a sea-ice floe," *J Eng Math*, 62, 355-372.

Kohout, AL, and Meylan, MH (2008). "An elastic plate model for wave attenuation and ice floe breaking in the marginal ice zone," *J Geophys Res*, 113, C09016.

Meylan, MH, Bennetts, LG, and Kohout, AL (2014). "In-situ measurements and analysis of ocean waves in the Antarctic marginal ice zone," *Geophys Res Lett*, 41, 5046-5051.

Milewski, PA, Vanden-Broeck, J-M, and Wang, Z (2011). "Hydroelastic solitary waves in deep water," *J Fluid Mech*, 679, 628-640.

Newyear, K, and Martin, S (1997). "A comparison of theory and laboratory measurements of wave propagation and attenuation in grease ice," *J Geophys Res*, 102, 25091-25099.

Părău, E, and Dias, F (2002). "Nonlinear effects in the response of a floating ice plate to a moving load," *J Fluid Mech*, 460, 281-305.

Părău, EI, and Vanden-Broeck, J-M (2011). "Three-dimensional waves beneath an ice sheet due to a steadily moving pressure," *Phil Trans R Soc A*, 369, 2973-2988.

Plotnikov, PI, and Toland, JF (2011). "Modelling nonlinear hydroelastic waves," *Phil Trans R Soc A*, 369, 2942-2956.

Tian, Z, and Choi, W (2013). "Evolution of deep-water waves under wind forcing and wave breaking effects: Numerical simulations and experimental assessment," *Eur J Mech B/Fluids*, 41, 11-22.

Wadhams, P, Squire, VA, Goodman, DJ, Cowan, AM, and Moore, SC (1988). "The attenuation rates of ocean waves in the marginal ice zone," *J Geophys Res*, 93, 6799-6818.

Wang, R, and Shen, HH (2010). "Gravity waves propagating into an ice-covered ocean: a viscoelastic model," *J Geophys Res*, 115, C06024.

Williams, TD, and Squire, VA (2004). "Oblique scattering of plane flexural-gravity waves by heterogeneities in sea-ice," *Proc R Soc A*, 460, 3469-3497.

Xu, L, and Guyenne, P (2009). "Numerical simulation of three-dimensional nonlinear water waves," *J Comp Phys*, 228, 8446-8466.

Zakharov, VE (1968). "Stability of periodic waves of finite amplitude on the surface of a deep fluid," *J Appl Mech Tech Phys*, 9, 190-194.

Zhao, X, Shen, HH, and Cheng, S (2015). "Modeling ocean wave propagation under sea ice covers," *Acta Mech Sinica*, 31, 1-15.